particular $Rh^I(CO)_2$ species may reflect the differences in reducing/oxidizing properties of these specific surface sites.

D. Agglomeration of Atomically Dispersed Rh^I. As discussed above the reduction of $Rh^I \rightarrow Rh^0$ and the subsequent aggregation in the presence of $H_2(g)$ occurs readily at $T \sim 200$ K and P_{H_2} as low as 10^{-1} Torr. The agglomerization is also kinetically controlled by the relative ratio of atomically dispersed (Rh^I) to crystallite (metallic Rh^0) sites as seen in Figure 11. This can be understood on the basis of our postulated mechanism above; the metallic Rh^0_x sites act as "feeder sites" for hydrogen atoms that induce the reductive agglomerization. With a higher loading of Rh/Al_2O_3 (10% Rh/Al_2O_3) these "feeder sites" are in close proximity to the isolated Rh^I sites. As a result the availability of migrating H atoms is considerably enhanced. On the other hand when almost no metallic Rh^0_x sites are present (0.2% Rh/Al_2O_3) this process is inhibited (Figure 11A).

V. Summary and Conclusions

On the basis of the results of this work, the following conclusions can be made: (1) A general phenomenon, common for OH groups on both Al_2O_3 and SiO_2, has been observed in which the reaction $(1/x)Rh^0_x + OH + 2CO(g) \rightarrow Rh^I(CO)_2 + (1/2)H_2(g)$ occurs. This reaction leads to a significant structural degradation of oxide-supported Rh catalysts. (2) The oxidation process above can be reversed by $H_2(g)$ addition to $Rh^I(CO)_2$ on either Al_2O_3 or SiO_2 supports. (3) The oxidation process in (1) above does not exhibit a deuterium kinetic isotope effect. (4) The H_2-induced reduction of $Rh^I(CO)_2$ to Rh^0_x depends upon the presence of Rh^0_x sites to provide H(ads) species in a spillover mechanism. (5) Direct spectroscopic evidence for the specific involvement of isolated surface OH groups in the oxidation of Rh^0_x sites to Rh^I sites has been obtained.

Acknowledgment. We acknowledge, with thanks, the support of this work by the Office of Basic Energy Sciences, DOE. One of us (P.B.) is grateful for a supported educational leave from Alcoa. Another (D.P.) acknowledges with thanks the support of the NSF Eastern European Program, Grant. No. INT-8513805.

Registry No. Rh, 7440-16-6; CO, 630-08-0.

Methoxyethylene Ozonide: Analysis of the Structure and Anomeric Effect by Microwave Spectroscopy and ab Initio Techniques[1]

Marabeth S. LaBarge,[‡] Helmut Keul,[†,‡] Robert L. Kuczkowski,*[‡] Markus Wallasch,[§] and Dieter Cremer*[§]

Contribution from the Department of Chemistry, The University of Michigan, Ann Arbor, Michigan 48109, and Lehrstuhl für Theoretische Chemie, Universität Köln, D-5000 Köln 41, Federal Republic of Germany. *Received July 8, 1987*

Abstract: Fifteen isotopic species of methoxyethylene ozonide (3-methoxy-1,2,4-trioxolane) were synthesized and their microwave spectra assigned. The dipole moment was determined as 1.99 (4) D. The structure was determined from the rotational constants by both least-squares (r_o) and Kraitchman substitution (r_s) methods. Methoxyethylene ozonide has a peroxy envelope ring conformation and an axial methoxy substituent with a short C–OCH_3 bond. The methoxy group exhibits an unusual orientation anti to the ring hydrogen placing it over the ozonide ring. Ab initio calculations were performed to provide additional insights on the structural features. Both experimental and theoretical results are in accord with the anomeric and exo-anomeric effects.

The anomeric effect is a stereoelectronic phenomenon[2,3] which influences molecular conformations[4,5] and reactivities[6-11] of a wide range of species. This effect refers to the preference of an electronegative substituent to adopt an axial rather than the sterically favored equatorial orientation in heterocyclic rings.[3] A related stereoelectronic effect is the exo-anomeric effect. It is defined as the preference of R in OR (alkoxy) substituents for a gauche orientation relative to the ring heteroatom (X) in R–X–C–OR moieties. The anomeric and exo-anomeric effects have the same electronic origin associated with two-electron interactions between antibonding orbitals and filled bonding or nonbonding orbitals.

Concomitant with these conformational tendencies are significant changes in bond lengths from "normal" based on simple inductive effects by electronegative substituents. Numerous X-ray crystallographic investigations of carbohydrates have revealed a lengthening of the exocyclic C–X bonds when X is halogen and shortening when X is oxygen. Jeffrey and Pople[12] and others[13-15] have used ab initio molecular orbital techniques to study carbohydrate related moieties in order to correlate theoretical and experimental structural data.

A number of experimental and theoretical studies of fluoro-ozonides and other substituted ozonides have also provided data

[†] Present address: Lehrstuhl für Textilchemie und Makromoleculare Chemie, der RWTH, Aachen, Federal Republic of Germany.
[‡] The University of Michigan.
[§] Universität Köln.

(1) Presented in part as paper TA5, 41st Symposium on Molecular Spectroscopy, The Ohio State University, Columbus, OH, 1986.
(2) For recent reviews, see: (a) *Anomeric Effect: Origin and Consequences*; Szarek, W. A., Horton, D., Eds.; American Chemical Society: Washington, DC, 1979; ACS Symp. Ser. No. 87. Kirby, A. J. *Anomeric Effect and Related Stereoelectronic Effects at Oxygen*; Springer-Verlag: Berlin, 1983. (c) Deslongchamps, P. *Stereoelectronic Effects in Organic Chemistry*; Pergamon Press: London, 1983.
(3) Lemieux, R. U.; Chu, N. J. *Abstracts of Papers*, 133rd National Meeting of the American Chemical Society, San Francisco, CA; American Chemical Society: Washington, DC, 1958; No. 31N.
(4) Eliel, E. L. *Angew. Chem., Int. Ed. Engl.* **1972**, *11*, 739.
(5) de Hoog, A. J.; Buys, H. R.; Altona, C.; Havinga, E. *Tetrahedron* **1969**, *25*, 3365.
(6) Malatesta, V.; Ingold, K. U. *J. Am. Chem. Soc.* **1981**, *103*, 609.
(7) Beckwith, A. L. J.; Easton, C. J. *J. Am. Chem. Soc.* **1981**, *103*, 615.
(8) Bailey, W. F.; Croteau, A. A. *Tetrahedron Lett.* **1981**, *22*, 545.
(9) McKelvey, R. D.; Iwamura, H. *J. Org. Chem.* **1985**, *50*, 402.
(10) Danishefsky, S.; Langer, M. E. *J. Org. Chem.* **1985**, *50*, 3672.
(11) Deslongchamps, P. *Tetrahedron* **1975**, *31*, 2463.
(12) (a) Jeffrey, G. A.; Pople, J. A.; Radom, L. *Carbohydr. Res.* **1972**, *25*, 117. (b) Jeffrey, G. A.; Pople, J. A.; Radom, L. *Ibid.* **1974**, *38*, 81. (c) Jeffrey, G. A.; Pople, J. A.; Binkley, J. S.; Vishveshwara, S. *J. Am. Chem. Soc.* **1978**, *100*, 373. (d) Jeffrey, G. A.; Yates, J. H. *J. Am. Chem. Soc.* **1979**, *101*, 820.
(13) Wolfe, S.; Whangbo, M.-H.; Mitchell, D. J. *Carbohydr. Res.* **1979**, *69*, 1.

0002-7863/88/1510-2081$01.50/0

on the anomeric effect in five-membered ring systems.[16-22] In parallel with carbohydrate–pyranose systems, the fluorine substituents in fluoroozonides were axially oriented, and the C–F bonds were some 0.03–0.04 Å longer than normal. This was rationalized by an anomeric interaction involving the fluorine atoms and the oxygens in the ring.

Although extensive structural investigations have been performed on carbohydrate systems,[23] far fewer structures have been reported for ring compounds such as 2-alkoxy-1,3-dioxolanes containing two endocyclic oxygen atoms bonded to a carbon bearing an alkoxy substituent.[24,25] This has precluded a correlation of endocyclic and exocyclic C–O bond lengths in such compounds. With the recent synthesis of the first alkoxy ozonide,[26] methoxyethylene ozonide (3-methoxy-1,2,4-trioxolane, MeO-Oz), the opportunity was provided to study a compound containing the O–C(OR)–O moiety. Insights from an investigation of the prototype MeO-Oz would have implications for 2-alkoxy-1,3-dioxolanes whose conformational equilibria have been extensively studied. It was also attractive to compare the structural parameters and anomeric effect between MeO-Oz and fluoroozonides and to complement a detailed microwave structural study of MeO-Oz with insights from ab initio calculations.

Experimental Section

Instrumentation. Microwave spectra were recorded in the range 26.5–40.0 GHz with a Hewlett-Packard 8460A Stark modulated spectrometer. Radio frequency microwave double resonance (RFMWDR) spectra of the a-type R-branch transitions ($K_p = 3$) were obtained with a tunable amplitude modulated radio frequency source from 1–20 MHz at 1–3 W output. All microwave data were collected with a PDP-11/23 computer interfaced to the spectrometer. Such signal averaging techniques enhanced the spectral sensitivity and resolution, especially for the low enriched isotopic species. Frequency measurements at pressures of 10–15 mTorr were accurate to ±0.02 MHz. The spectrometer cells were cooled with dry ice to between −30 to −40 °C and preconditioned with the sample. This increased the decomposition half-life of MeO-Oz to typically 15–20 min.

Theoretical Methods. Complete geometry optimizations of MeO–Oz have been carried out at the Hartree–Fock (HF)/STO-3G and the HF/4-31G level of theory[27] employing a newly developed program for calculating analytic energy gradients for puckered rings.[28] This is based on the use of the ring puckering coordinates (puckering amplitudes q and pseudorotation phase angles ϕ) defined by Cremer and Pople.[29] The ring puckering coordinates are the appropriate internal coordinates to assess the degree and mode of ring puckering, to quantitatively relate different ring conformations, to describe conformational processes in ring molecules, and to determine ring substituent positions.[29,30]

In order to assess couplings between conformational modes of the ozonide ring (pseudorotation) and those of the MeO substituent (rotation at the C–OMe and the CO–Me bond), geometry optimizations for nine fixed values of the dihedral angle τ(HC–OMe) = τ have been carried out at the HF/STO-3G level. Investigation of the molecular energy dependence of τ suggested three rotational minima **1**, **2**, and **3**. These

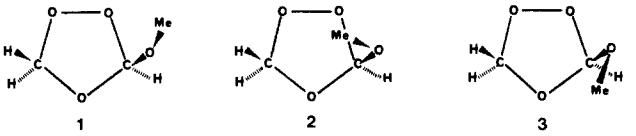

1 2 3

60° (exo Me) 180° (endo Me) −60° (exo Me)

minima have been confirmed (a) by complete geometry optimizations including q, ϕ, and τ (33 geometrical variables) at the HF/STO-3G level and (b) by repeating these calculations at the HF/4-31G level.

For the most stable MeO-Oz conformation a single-point HF/6-31G*//HF/4-31G calculation has been carried out in order to investigate electronic and steric interactions between the MeO substituent and the ozonide ring. For this purpose, molecular orbitals (MO), the total electron distribution $\rho(\mathbf{r})$, and its associated Laplace field $\nabla^2\rho(\mathbf{r})$ have been analyzed by using the program COLOGNE,[31] which contains large parts of GAUSSIAN 82.[32]

Syntheses. In previous papers the synthesis and purification of MeO-Oz from the ozonolysis of styrene[26] or methyl vinyl ether[33] in methyl formate were reported. Since both of these reactions also produced inseparable volatile impurities which gave interfering lines in the microwave spectrum, a new synthesis was developed. Typically, 1–5 mmol of *p*-nitro-α-ethoxystyrene[34] (**4**) were ozonized to completion in 2–8 mL

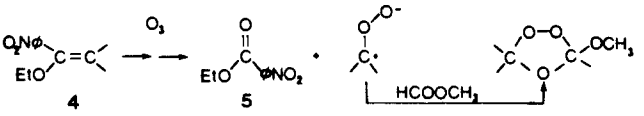

4 5

of $HCOOCH_3$ at −78 °C to give MeO-Oz and an involatile ester residue, ethyl *p*-nitrobenzoate (**5**). A slow ozone flow rate of 0.04–0.08 mmol/min O_3 in O_2 was used. After ozonolysis, the solution was warmed to 25 °C and MeO-Oz and $HCOOCH_3$ were separated from **5** by distillation through a −196 °C trap with an active vacuum. MeO-Oz was separated from the solvent by two successive distillations through traps held at −41 °C and −196 °C. The purified ozonide was collected from the −41 °C traps and stored under vacuum at −196 °C. Methyl formate comprised less than 1% of the purified ozonide sample as determined by NMR and microwave spectroscopy.

Isotopically labeled species were prepared from labeled ozone, labeled methyl formate, and/or labeled **4** except for MeO–Oz-*cis*-d_1 and MeO–Oz-*trans*-d_1 which were made from deuteriated styrene. Labeled ozone was produced by the electric discharge of $^{18}O_2/^{16}O_2$ mixtures (97.8% $^{18}O_2$, Monsanto) in the static ozone generator previously described.[17,35] Standard techniques were employed to synthesize about 1–2 mL of various labeled methyl formate species in >50% enrichment. All samples were dried and purified from methanol prior to ozonolyses by reaction with and distillation from P_2O_5. Enrichments were determined by microwave relative intensity measurements.

Isotopic Species. **MeO-Oz-OCD$_3$** ($\overline{CH_2OOCH(OCD_3)O}$) (>99%) was synthesized by ozonolysis in methyl formate-d_3. $HCOOCD_3$ was prepared from the acid-catalyzed esterification of methanol-d_4 (>99.5% D, Aldrich) and formic acid.[36]

MeO-Oz-*cis*-d_1 ($\overline{CHDOOCH(OCH_3)O}$) (80%) and **MeO-Oz-*trans*-d_1** ($\overline{CDHOOCH(OCH_3)O}$) (80%) were made from (*E*)-styrene-β-d_1 and (*Z*)-styrene-β-d_1, respectively. The starting materials and synthesis of labeled styrene were previously reported.[37,38] The labeled styrene used

(14) Tvaroška, I.; Kozar, T. *J. Am. Chem. Soc.* **1980**, *102*, 6929.
(15) (a) Schäfer, L.; Van Alsenoy, C.; Williams, J. O.; Scarsdale, J. N.; Geise, H. J. *J. Mol. Struct.* **1981**, *76*, 349. (b) Williams, J. O.; Scarsdale, J. N.; Schäfer, L.; Geise, H. J. *Ibid.* **1981**, *76*, 11. (c) Van Nuffel, P.; Van Alsenoy, C.; Lenstra, A. T. H.; Geise, H. J. *Ibid.* **1984**, *125*, 1.
(16) LaBarge, M. S.; Hillig, II, K. W.; Kuczkowski, R. L.; Cremer, D. *J. Phys. Chem.* **1986**, *90*, 3092.
(17) Hillig, II, K. W.; Lattimer, R. P.; Kuczkowski, R. L. *J. Am. Chem. Soc.* **1982**, *104*, 988.
(18) Hillig, II, K. W.; Kuczkowski, R. L. *J. Phys. Chem.* **1982**, *86*, 1415.
(19) Hillig, II, K. W.; Kuczkowski, R. L.; Cremer, D. *J. Phys. Chem.* **1984**, *88*, 2025.
(20) Cremer, D. *J. Am. Chem. Soc.* **1981**, *103*, 3633.
(21) Cremer, D. *J. Chem. Phys.* **1979**, *70*, 1928.
(22) Cremer, D. *J. Chem. Phys.* **1979**, *70*, 1898.
(23) For a complete index of structural data and references for carbohydrates, nucleosides, and nucleotides based on chemical formulas in the Cambridge Crystallography Data Bank, see: Jeffrey, G. A.; Sundaralingam, M. *Adv. Carbohydr. Chem. Biochem.* **1985**, *43*, 203.
(24) (a) Heitmann, J. A.; Richards, G. F. *Carbohydr. Res.* **1973**, *28*, 180. (b) Heitmann, J. A.; Richards, G. F.; Schroeder, L. R. *Acta Crystallogr., Sect. B: Struct. Crystallogr. Cryst. Chem.* **1974**, *B30*, 2322.
(25) Bunnelle, W. H.; Schlemper, E. O. *J. Am. Chem. Soc.* **1987**, *109*, 612.
(26) Keul, H.; Kuczkowski, R. L. *J. Am. Chem. Soc.* **1984**, *106*, 3383.
(27) *STO-3G*: Hehre, W. J.; Stewart, R. F.; Pople, J. A. *J. Chem. Phys.* **1969**, *51*, 2657. *4-31G*: Ditchfield, R.; Hehre, W. J.; Pople, J. A. *J. Chem. Phys.* **1971**, *54*, 724. *6-31G**: Hariharan, P. C.; Pople, J. A. *Theor. Chim. Acta* **1973**, *28*, 213.
(28) Cremer, D.; Wallasch, M., to be published.
(29) Cremer, D.; Pople, J. A. *J. Am. Chem. Soc.* **1975**, *97*, 1354.
(30) (a) Cremer, D. *Isr. J. Chem.* **1980**, *20*, 12. (b) Cremer, D. *Fresenius Z. Anal. Chem.* **1980**, *304*, 275. (c) Essén, H.; Cremer, D. *Acta Crystallogr., Sect. B: Struct. Sci.* **1984**, *B40*, 418. (d) Cremer, D. *Acta Crystallogr., Sect. B: Struct. Sci.* **1984**, *B40*, 498.
(31) Gauss, J.; Kraka, E.; Cremer, D. COLOGNE 87, Universität Köln, 1987.
(32) Binkley, J. S.; Frisch, M. J.; DeFrees, D. J.; Raghavachari, K.; Whiteside, R. A.; Schlegel, H. B.; Fluder, E. M.; Pople, J. A. GAUSSIAN 82, Carnegie-Mellon University: Pittsburgh, PA, 1985.
(33) Keul, H.; Kuczkowski, R. L. *J. Am. Chem. Soc.* **1984**, *106*, 5370.
(34) Hanzlik, R. P.; Hilbert, J. M. *J. Org. Chem.* **1978**, *43*, 610.
(35) Lopata, A. D.; Kuczkowski, R. L. *J. Am. Chem. Soc.* **1981**, *103*, 3304.
(36) Buehler, C. A.; Pearson, D. E. *Survey of Organic Syntheses*; Wiley Interscience: New York, 1970; Vol. 1, p 802.

here was obtained from that work. The ozonides obtained were 80% cis:20% trans from the (*E*)-styrene and 80% trans:20% cis from the (*Z*)-styrene.[39]

MeO-Oz-*gem*-d_1 ($\overline{CH_2OOCD(OCH_3)O}$) (99%) was prepared from $DCOOCH_3$ made from the acid-catalyzed esterification of formic acid-d_1 (99% D, MSD Isotopes) and methanol.

MeO-Oz-*5,5*-d_2 ($\overline{CD_2OOCH(OCH_3)O}$) (99%) was made from the ozonolysis of *p*-nitro-α-ethoxystyrene-d_2 in methyl formate. *p*-Nitro-α-ethoxystyrene-d_2 was prepared from *p*-nitroacetophenone by analogy to methods described in the literature.[34] The starting materials (Aldrich) were *p*-nitroacetophenone, D_2O (99% D), and triethyl orthoformate. *p*-Nitroacetophenone-d_3 was prepared by exchange of the normal species with acetic acid-d_1 (CH_3COOD) at 130 °C for 24 h. Ethanol-d_1 (CH_3CH_2OD) was prepared from D_2O in excess triethyl orthoformate. *p*-Nitroacetophenone-d_3 was refluxed in the triethyl orthoformate and ethanol-d_1 solution producing *p*-nitroacetophenone dimethyl ketal which was then converted to *p*-nitro-α-ethoxystyrene-d_2 for ozonolysis.

MeO-Oz-*3,5,5*-d_3 ($\overline{CD_2OOCD(OCH_3)O}$) (99%) was made from the ozonolysis of *p*-nitro-α-ethoxystyrene-d_2 in $DCOOCH_3$.

MeO-Oz-$^{18}O_p$-$^{18}O_p$ ($\overline{CH_2{}^{18}O{}^{18}OCH(OCH_3)O}$) (98%) was made from 97.8% $^{18}O_3$ and methyl formate.

MeO-Oz-$^{18}O_p$(C_H) ($\overline{CH_2{}^{18}OOCH(OCH_3)O}$), **MeO-Oz-$^{18}O_p$($C_{methoxy}$)** ($\overline{CH_2O{}^{18}OCH(OCH_3)O}$), **MeO-Oz-$^{18}O_p$-$^{18}O_p$**, and *n*-MeO-Oz were produced simultaneously from labeled ozone (40% ^{18}O, 60% ^{16}O) and unlabeled methyl formate. Their relative intensities were consistent with the expected enrichment ratios of 24%, 24%, 16%, and 36%, respectively.

MeO-Oz-$^{18}O_e$ ($\overline{CH_2OOCH(OCH_3)^{18}O}$) (50%) was prepared by using $HC^{18}OOCH_3$ (50% ^{18}O) which was made from the acid-catalyzed hydrolysis (97.3% $H_2{}^{18}O$, MSD Isotopes) of trimethyl orthoformate.[40] Dry HCl gas and anhydrous diglyme solvent were used in this synthesis to minimize dilution of the isotopic enrichment.

MeO-Oz-$^{18}O_3$(*ring*) ($\overline{CH_2{}^{18}O{}^{18}OCH(OCH_3)^{18}O}$) (50%) was made from labeled ozone (97.8% $^{18}O_2$, Monsanto) and $HC^{18}OOCH_3$ (50% ^{18}O).

MeO-Oz-$^{18}O_{methoxy}$ ($\overline{CH_2OOCH(^{18}OCH_3)O}$) (50%) was made from $HCO^{18}OCH_3$ (50% ^{18}O) prepared by the acid-catalyzed esterification of formic acid with ^{18}O labeled methanol. $CH_3{}^{18}OH$ (50% ^{18}O) was made by diluting 1.0 g of $CH_3{}^{18}OH$ (95% ^{18}O, Cambridge Isotopes) with an equimolar amount of unlabeled CH_3OH.

MeO-Oz-$^{13}C_{ring}$(*OCH*$_3$) ($\overline{CH_2OO{}^{13}CH(OCH_3)O}$) (50%) was prepared by using $H^{13}COOCH_3$ (50% ^{13}C) obtained by diluting 1.0 g of $H^{13}COOCH_3$ (99% ^{13}C, ICON Services) with an equimolar amount of unlabeled methyl formate.

MeO-Oz-$^{13}C_{methoxy}$ ($\overline{CH_2OOCH(O{}^{13}CH_3)O}$) (75%) was made from methyl formate-methoxy-^{13}C (75% ^{13}C) prepared by the acid-catalyzed esterification of formic acid with ^{13}C labeled methanol. The latter was obtained by diluting 1.0 g of $^{13}CH_3OH$ (99% ^{13}C, Cambridge Isotopes) with 0.350 g of CH_3OH.

Spectra. The spectrum was characteristic of a near prolate asymmetric top with $\kappa = -0.92$ and μ_a, μ_b, and μ_c selection rules. This resulted in prominent degenerate μ_b and μ_c Q-branch series with band origins roughly at intervals of $(A - (B + C)/2)$ $(2K + 1)$ and μ_a R-branch clusters separated by $(B + C)$. The spectral regions between these intervals were generally sparse except for occasional unassigned lines which had weak-to-moderately strong intensities. Several series of vibrational satellites accompanied each ground state Q-branch series on the high frequency side.

The initial assignment began with rigid rotor fits of high-J ($J > 10$) $K_p = 6 \rightarrow 7$ Q-branch transitions after carefully testing the assignment by shifting up and down in J. These fits were used to predict and measure Q-branch transitions for two other series in the accessible spectral region. Centrifugal distortion fits were then performed by using the program ZFAP6.[41] The Q-branch transitions were fit to A–C, κ, and several fourth-order centrifugal distortion constants. The fit with the smallest root-mean-square (rms) deviation was assumed to be correct. Next, calculated values of A–C and κ for various model conformations of MeO-Oz were plotted versus τ in 20° increments to determine the orientation of the methoxy group. The model having an axial methoxy substituent and methyl group over the ring was in best agreement with the experimental Q-branch data. By using the predicted A rotational constant from this model and the values of A–C and κ from the best Q-branch fit, the μ_a R-branch $K_p = 3$ K-doublet transitions were predicted and found by using RFMWDR. Utilizing all the experimental data to obtain good estimates of A, B, and C, the remaining μ_a and weaker μ_b and μ_c R-branch transitions could then be assigned guided by their relative intensities and Stark effects.

A centrifugal distortion fit for 109 transitions (representing 57 uniquely resolvable lines) of the parent isotopic species was performed. The rms deviation was 59 kHz for the quartic fit to three rotational constants and five centrifugal distortion constants using the Watson-S reduction, representation I^r. A selection of the assigned transitions is given in Table I. Centrifugal distortion effects are small with the largest deviation from a rigid rotor model of about 3 MHz for a $J = 20 \rightarrow 20$ transition. The rotational constants and centrifugal distortion constants for *n*-MeO-Oz are listed in Table I. No internal rotation splittings from the methyl group were observed.

The assignment of the isotopic species also commenced with Q-branch centrifugal distortion fits. The values of A–C and κ were then used in a modified version of the STRFIT structure-fitting program[42] to bootstrap toward an improved structure which in turn aided in R-branch predic-

Table I. Assigned Rotational Transitions of the Normal Isotopic Species of MeO-Oz

transition	ν(obsd), MHz	ν(calcd) − ν(obsd)[a]
5(2,4)–4(1,3)	30 652.83	0.038
5(3,3)–4(2,3)	36 027.68	0.169
5(3,2)–4(2,2)	35 984.31	−0.170
6(1,6)–5(0,5)	30 084.18	0.044
6(0,6)–5(0,5)	28 531.18	0.008
6(1,6)–5(1,5)	28 314.26	−0.085
6(1,5)–5(1,4)	28 906.08	0.052
7(1,7)–6(0,6)	34 576.09	−0.006
7(1,6)–6(0,6)	37 341.44	−0.040
7(0,7)–6(0,6)	33 245.14	−0.027
7(2,6)–6(2,5)	33 383.11	0.017
7(2,5)–6(2,4)	33 544.47	−0.066
7(3,5)–6(3,4)	33 428.55	−0.070
7(3,4)–6(3,3)	33 435.61	0.123
7(4,X)–6(4,X)[b]	33 421.98	0.050
7(5,X)–6(5,X)	33 417.91	−0.047
7(6,X)–6(6,X)	33 415.81	−0.006
8(0,8)–7(1,7)	33 613.15	0.170
8(1,7)–7(2,5)	32 193.24	0.152
8(1,8)–7(0,7)	39 058.95	−0.031
8(0,8)–7(0,7)	37 944.31	−0.019
8(1,8)–7(1,7)	37 728.06	−0.112
8(2,7)–7(2,6)	38 141.66	0.059
9(0,9)–8(1,7)	37 970.90	0.120
10(6,X)–10(5,X)[b,c]	26 695.51	−0.020[d]
11(6,X)–11(5,X)	26 686.95	0.052
12(7,X)–12(6,X)	31 548.85	0.009
13(7,X)–13(6,X)	31 540.65	0.039
15(7,X)–15(6,X)	31 517.61	0.026
16(7,X)–16(6,X)	31 501.98	0.046
26(7,20)–26(6,21)	31 098.83	0.047
26(7,19)–26(6,20)	31 063.99	−0.053
12(8,X)–12(7,X)	36 413.36	0.000
15(8,X)–15(7,X)	36 394.15	0.018
18(8,X)–18(7,X)	36 358.75	0.010
19(8,X)–19(7,X)	36 342.17	−0.022
20(8,X)–20(7,X)	36 322.63	−0.022

[a] Calculated from a centrifugal distortion fit of 109 transitions. [b] X denotes both values of K_o where $K_o = J - K_p$ and $K_o = J + 1 - K_p$. [c] Each transition represents four μ_b and μ_c Q-branch lines which were not resolvable. [d] Differences listed for the nearly degenerate transitions are the average of the four calculated differences.

(37) Keul, H.; Kuczkowski, R. L. *J. Org. Chem.* **1985**, *50*, 3371.
(38) Wood, J. T.; Arney, J. S.; Cortès, D.; Berson, J. A. *J. Am. Chem. Soc.* **1978**, *100*, 3855.
(39) The stereoassignment of the *cis*- and *trans*-d_1 isotopes of MeO-Oz is unambiguous from their isotopic shifts in the microwave spectrum. This supports the ^1H NMR assignment for alkoxy ozonides determined in the investigation of the stereochemistry of 1,3-dipolar cycloaddition reactions of HDCOO, ref 37.
(40) Sawyer, C. B.; Kirsch, J. F. *J. Am. Chem. Soc.* **1973**, *95*, 7375.
(41) (a) Van Eijck, B. P. *J. Mol. Spectrosc.* **1974**, *53*, 246. (b) Typke, V. *J. Mol. Spectrosc.* **1976**, *63*, 170. (c) Watson, J. K. G. In *Vibrational Spectra and Structure*; Durig, J. R., Ed.; Elsevier: 1977; Vol 6.
(42) Schwendeman, R. H. In *Critical Evaluation of Chemical and Physical Structural Information*; Lide, D. R., Paul, M. A., Eds.; National Academy of Sciences: Washington, DC, 1974; pp 74–115.

Table II. Rotational Constants of Isotopic Species of MeO-Oz[a]

species	A, MHz	B, MHz	C, MHz	no. of assigned transtns	rms deviatn of fit, MHz
normal[b]	4815.386 (3)	2435.852 (3)	2336.675 (3)	109	0.059
OCD_3	4528.946 (4)	2261.995 (5)	2194.380 (5)	110	0.036
gem-d_1	4649.811 (4)	2402.231 (4)	2324.870 (4)	92	0.035
trans-d_1	4796.858 (9)	2369.006 (10)	2271.515 (8)	79	0.043
cis-d_1	4697.108 (8)	2371.327 (8)	2294.791 (8)	96	0.038
5,5-d_2	4679.612 (4)	2307.999 (4)	2233.467 (4)	119	0.035
3,5,5-d_3	4522.546 (4)	2274.161 (4)	2225.200 (4)	120	0.028
$^{18}O_p$-$^{18}O_p$	4607.487 (3)	2379.745 (4)	2273.670 (3)	133	0.031
$^{18}O_e$	4692.028 (6)	2430.848 (7)	2303.247 (7)	101	0.058
$^{18}O_p(C_H)$	4729.661 (15)	2401.479 (19)	2290.611 (14)	53	0.073
$^{18}O_p(C_{methoxy})$	4686.973 (9)	2416.213 (10)	2315.558 (12)	73	0.074
$^{18}O_3$(*ring*)	4486.042 (6)	2376.398 (6)	2240.697 (7)	96	0.055
$^{18}O_{methoxy}$	4800.077 (7)	2376.054 (7)	2283.027 (8)	104	0.054
$^{13}C_{methoxy}$	4771.800 (8)	2389.909 (8)	2301.067 (8)	110	0.073
$^{13}C_{ring}(OCH_3)$	4782.944 (7)	2428.425 (8)	2334.265 (8)	78	0.061

[a] Uncertainties in parentheses represent one standard deviation in the fit. [b] The centrifugal distortion constants (in kHz) for the normal species are D_J = 0.801 (25), D_{JK} = −1.403 (9), D_K = 3.389 (37), d_1 = 0.077 (4), d_2 = −0.033 (5).

tions and assignments. For all isotopically labeled species, at least two pairs of μ_a R-branch K_p = 3 transitions had to be identified by using RFMWDR to guarantee an unambiguous assignment. The assignments of the species which were enriched to at least 50% were simplified by using signal averaging techniques to follow Stark effects and to find RFMWDR transitions. The assignment of the $^{18}O_p(C_H)$ and $^{18}O_p$-($C_{methoxy}$) species which were 25% enriched proved to be more difficult. For these species, the centrifugal distortion constants were fixed at the normal species values enabling the *A*, *B*, and *C* rotational constants to be determined from two RFMWDR K_p = 3 R-branch and the Q-branch transitions. This predicted the remaining R-branch transitions within 1 MHz. Rotational constants for all the isotopic species are given in Table II. A complete list of the assigned transitions and centrifugal distortion constants for all isotopic species is available (Tables S1–S16, Supplementary Material.) An inspection of the distortion constants for the 14 species shows them to have similar signs and magnitudes. This served as an important criterion is evaluating the spectral assignments of the isotopic species.

Dipole Moment. The second-order Stark effects for the M = 1 components of five transitions were measured. The values of $\Delta\nu/E^2$ were typically determined at two to four electric field values. The richness of the spectrum precluded the tracking of Stark lobes over further distances. A least-squares fit of $\Delta\nu/E^2$ using the calculated second-order Stark coefficients resulted in the dipole components μ_a = 1.527 (10) D, μ_b = 0.522 (60) D, μ_c = 1.169 (30) D, and μ_{total} = 1.993 (40) D. These Stark coefficients are available (Table S17, Supplementary Material). There is good agreement (±1%) between the observed and calculated values of $\Delta\nu/E^2$ except for M = 1 of the 7(2,6)–6(2,5) transition which differ by 9%. The reason for this discrepancy is unclear. No other low-J transitions with resolved Stark effects could be measured between 26.5–40 GHz to supplement the existing data. The electric field was calibrated with the J = 2 → 3, M = 2 transition of OCS at 36 488.814 MHz.[43]

Structure. Since MeO-Oz has no elements of symmetry, 3N = 39 atomic coordinates equivalent to 3N-6 internal coordinates are needed to define the structure. In principle, the coordinates can be calculated by using either a standard least-squares fitting of observed moments of inertia (r_o method) or by using Kraitchman's equations (r_s method).

The available data set consisted of 30 moments of inertia from the normal and single-substituted species, 18 moments of inertia from multiple-substituted species, three first moment equations ($\sum m_i a_i = 0$, etc.), and three product of inertia equations ($\sum m_i a_i b_i = 0$, etc). Because the multiply substituted species do not always provide independent inertial data and because no isotopic data are available to locate C_3, H_{11}, H_{12}, and H_{13}, a few structural assumptions were included to utilize the method of predicate observables or diagnostic least-squares.[44] (See Figures 1 and 2 for the numbering of the atoms.) The assumptions included C_3–H_9, C_3–H_{10}, and methyl C–H distances of 1.090 Å, bond angles about the methyl group of 109.47°, and a C_1, H_{13} nonbonded distance of 2.665 Å which is virtually identical with the value 2.664 determined by ab initio methods (see below). This latter constraint inhibited the methyl group from freely rotating in the fitting process and facilitated convergence. When this assumption was varied from 2.515 to 2.915 Å, it did not affect the final structure except for the methyl hydrogen torsional angles. It was also found that the removal of the moments of inertia of the OCD_3 species improved the rms deviation between observed and calculated parameters from 0.0112 to 0.0049 amu Å^2. It seems probable that triple deuteriation has significantly changed the vibrational amplitudes in the methoxy group, degrading the fitting

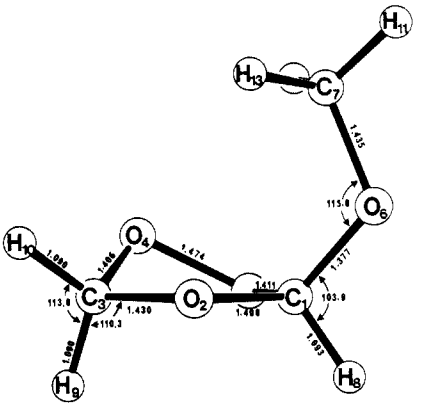

Figure 1. Structure of MeO-Oz, peroxy envelope conformation.

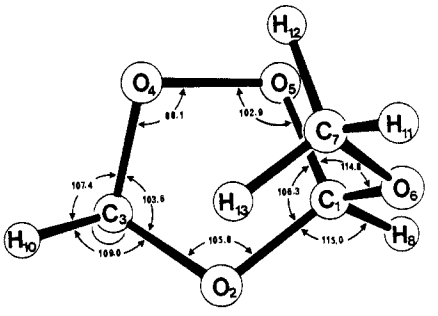

Figure 2. Structure of MeO-Oz, projection from top of ring.

Table III. Principal Axis Coordinates (Å) of MeO-Oz

atom	a_o[a]	a_s[b]	b_o[a]	b_s[b]	c_o[a]	c_s[b]
C_1	−0.2903	−0.2701	−0.3773	−0.3764	0.7617	0.7583
O_2	0.4425	0.4467	−1.1798	−1.1800	−0.1487	−0.1259
C_3	1.6023	1.6023	−0.4195	−0.4195	−0.4926	−0.4926
O_4	1.1629	1.1626	0.9139	0.9115	−0.3954	−0.4017
O_5	0.4389	0.4402	0.8305	0.8295	0.8836	0.8826
O_6	−1.5892	−1.5894	−0.2365	−0.2252	0.3596	0.3567
C_7	−1.7840	−1.7832	0.3929	0.3867	−0.9227	−0.9181
H_8	−0.3587	−0.3582	−0.8140	−0.8154	1.7583	1.7575
H_9	2.4127	2.4129	−0.6273	−0.6317	0.2058	0.1748
H_{10}	1.8446	1.8446	−0.6102	−0.6076	−1.5378	−1.5381

[a] From least-squares fit of inertial equations and assumed structural parameters described in text. [b] Kraitchman single substitution except for C_3, H_8, H_9, and H_{10}, see text.

(43) Muenter, J. S. *J. Chem. Phys.* **1968**, *48*, 4544.

(44) (a) Bartell, L. S.; Romanesko, D.; Wong, T. C. *Spec. Period. Rep.: Mol. Struct. Diffr. Methods* **1975**, *3*, Chapter 4. (b) Nösberger, P.; Bauder, A.; Günthard, Hs. H. *Chem. Phys.* **1973**, *1*, 418. (c) Kierns, J. J.; Curl, R. F., Jr. *J. Chem. Phys.* **1968**, *48*, 3773.

Table IV. Selected r_0 and r_s Structural Parameters of MeO-Oz from Coordinates in Table III

param[a]	r_0	r_s[b]	param[a]	r_0	r_s[b]
C_1–O_2	1.418 (8)[c]	1.394 (7)[d]	$\angle C_1$–O_2–C_3	105.8 (4)	105.8 (3)
C_1–O_5	1.416 (9)	1.406 (5)	$\angle O_2$–C_3–O_4	103.5 (3)	103.6 (2)
C_1–O_6	1.367 (7)	1.387 (6)	$\angle C_3$–O_4–O_5	99.2 (2	99.0 (2)
C_7–O_6	1.442 (5)	1.427 (5)	$\angle O_4$–O_5–C_1	103.1 (3)	102.6 (2)
C_3–O_4	1.407 (5)	1.406 (4)	$\angle O_5$–C_1–O_2	105.8 (5)	106.9 (4)
C_3–O_2	1.429 (5)	1.430 (4)	$\angle O_2$–C_1–O_6	111.1 (5)	111.6 (4)
O_4–O_5	1.472 (4)	1.474 (4)	$\angle O_5$–C_1–O_6	115.3 (7)	114.4 (4)
$\tau(C_3$–O_4–O_5–$C_1)$	−44.2	−43.8	$\tau(O_2$–C_1–O_6–$C_7)$	−60.7	−60.8
$\tau(O_4$–O_5–C_1–$O_6)$	−97.1	−97.6	$\tau(O_5$–C_1–O_2–$C_3)$	1.8	1.1

[a] Bond distances in Å and bond angles in deg. See Figure 1 and 2 for numbering of atoms. [b] Kraitchman single substitution using r_0 coordinates of C_3, 109.47° angles about the methyl group, and C–H bonds of 1.090 Å. [c] Uncertainty from propagation of coordinate uncertainties from the least-squares fitting. [d] Uncertainty from propagation of the Costain uncertainties (0.0015 Å/x_s) in the coordinates.

Table V. Structural Parameters of MeO-Oz from Spectroscopic[a] and ab Initio[b] Analysis

		ab initio[b] conformer					ab initio[b] conformer			dihedral		ab initio[b] conformer		
bond	spectrosc[a]	2	1	3	angle	spectrosc[a]	2	1	3	angle	spectrosc[a]	2	1	3
C_1–O_2	1.406 (20)	1.421	1.398	1.421	C_1–O_2–C_3	105.8 (4)	110.0	109.2	108.9	C_1–O_2–C_3–O_4	−30.2	−22.1	−4.1	−9.7
C_1–O_5	1.411 (14)	1.448	1.435	1.414	O_2–C_3–O_4	103.6 (4)	103.5	104.7	104.2	O_2–C_3–O_4–O_5	44.9	37.8	27.6	31.2
C_1–O_6	1.377 (17)	1.359	1.370	1.371	C_3–O_4–O_5	99.1 (3)	101.5	102.7	102.3	C_3–O_4–O_5–C_1	−44.0	−40.8	−40.8	−42.1
C_7–O_6	1.435 (13)	1.443	1.438	1.438	O_4–O_5–C_1	102.9 (5)	104.5	102.3	103.1	O_4–O_5–C_1–O_2	26.3	27.2	38.3	35.9
C_3–O_4	1.406 (6)	1.433	1.442	1.438	O_5–C_1–O_2	106.3 (10)	103.4	103.8	104.0	O_5–C_1–O_2–C_3	1.4	−3.5	−21.7	−16.7
C_3–O_2	1.430 (6)	1.423	1.431	1.429	O_2–C_1–O_6	111.4 (8)	112.8	109.2	112.0	C_3–O_2–C_1–O_6	127.2	119.9	98.3	101.8
O_4–O_5	1.474 (8)	1.467	1.466	1.466	O_5–C_1–O_6	114.8 (12)	113.8	112.4	109.8	O_4–O_5–C_1–O_6	−97.4	−95.5	−79.5	−84.1
C_1–H_8	1.093 (9)	1.069	1.074	1.074	C_1–O_6–C_7	115.8 (4)	120.6	118.1	117.9	O_2–C_1–O_6–C_7	−60.7	−56.3	−178.4	64.5
C_3–H_9	1.090[c]	1.074	1.073	1.073	O_2–C_1–H_8	113.0 (9)	111.5	111.0	109.2	O_5–C_1–O_6–C_7	60.0	61.1	63.9	179.5
C_3–H_{10}	1.090[c]	1.071	1.071	1.071	O_2–C_3–H_{10}	109.0 (9)	110.2	110.8	110.9	C_3–O_2–C_1–H_8	−116.2	−118.0	−135.4	−131.7
C_7–H_{11}	1.090[c]	1.074	1.074	1.074	O_2–C_3–H_9	110.3 (5)	110.7	109.2	109.6	C_1–O_2–C_3–H_{10}	−144.2	−137.5	−119.6	−125.1
C_7–H_{12}	1.090[c]	1.077	1.083	1.078	O_5–C_1–H_8	107.5 (9)	106.9	106.2	107.9	C_1–O_2–C_3–H_9	90.0	96.3	114.4	108.8
C_7–H_{13}	1.090[c]	1.078	1.078	1.082	O_4–C_3–H_9	112.1 (10)	110.5	110.7	110.7	O_4–O_5–C_1–H_8	147.6	145.0	155.4	151.9
					O_4–C_3–H_{10}	107.4 (5)	108.1	107.4	107.5	O_5–O_4–C_3–H_{10}	160.1	154.6	145.4	149.0
					H_9–C_3–H_{10}	113.9 (12)	113.4	113.7	113.5	O_5–O_4–C_3–H_9	−74.1	−80.8	−89.9	−86.6
					O_6–C_1–H_8	103.9 (13)	108.3	113.8	113.7	C_1–O_6–C_7–H_{11}	179.5	178.7	178.0	178.2
					O_6–C_7–H_{11}	109.47[c]	105.0	105.6	105.6	C_1–O_6–C_7–H_{12}	−59.5	−62.3	−59.4	−62.4
					O_6–C_7–H_{12}	109.47[c]	110.3	110.6	110.4	C_1–O_6–C_7–H_{13}	60.5	60.0	62.7	59.5
					O_6–C_7–H_{13}	109.47[c]	110.2	110.4	110.5	H_8–C_1–O_6–$C_7(\tau)$	177.3	179.8	56.9	−59.7

[a] The average of the results in Table IV with uncertainties sufficient to encompass both calculations. Uncertainties in the dihedral angles are ±1°. Bond distances in Å and bond angles in deg. See Figures 1 and 2 for illustrations with spectroscopic parameters. [b] HF/4-31G geometry. Conformers 1, 2, and 3 are illustrated in the Experimental Section. Conformer 2 is the lowest energy conformer (Table VI). [c] Assumed value.

process. The quality of the final r_0 fit was good (excluding the CD_3 data) with the largest difference between observed and calculated moments being 0.01 amu Å^2. The r_0 coordinates calculated from the least-squares fit are given in Table III. Selected structural parameters for MeO-Oz obtained from these coordinates are listed in Table IV.[45]

From the inertial data of nine singly substituted isotopic species, the substitution coordinates were calculated by using Kraitchman's equations and listed in Table III. There is reasonable agreement between the r_0 and r_s coordinates except for the *a* coordinate of C_1, the *b* coordinate of O_6, and the *c* coordinates of O_2 and H_9. These four differences range from 0.01 to 0.03 Å which most likely result from the Kraitchman method's underestimation of the small coordinates of these atoms.[46] Although the r_0 method is probably more reliable in determining small coordinates, its accuracy (i.e., extent of vibration–rotation interactions) cannot be determined without a vibrational analysis.

Insufficient isotopic data are available to completely determine the structure by the Kraitchman method since C_3, H_{11}, H_{12}, and H_{13} single substitution data are not available. To generate a partial r_s structure, the r_0 coordinates for C_3 and the available r_s coordinates were used. The methyl hydrogen coordinates were calculated by assuming tetrahedral geometry with C–H distances of 1.090 Å. This partial r_s structure is given in Table IV. There are significant differences between several of the r_0 and r_s structural parameters. For example, the C_1–O_2 and C_1–O_6 bond distances differ by 0.024 and 0.020 Å, respectively.

In view of the differences between the parameters computed by the two methods and the parameter uncertainties obtained by propagation of the coordinate uncertainties (see Table IV), we believe the average of these two structures (Table V) with uncertainties that encompass both calculations is the best way to report the structure of MeO-Oz. Although the physical relevance of the preferred structure in Table V is no longer clear, the parameters have generous uncertainties which most likely encompass the equilibrium structure. The structure of MeO-Oz is shown in Figures 1 and 2.

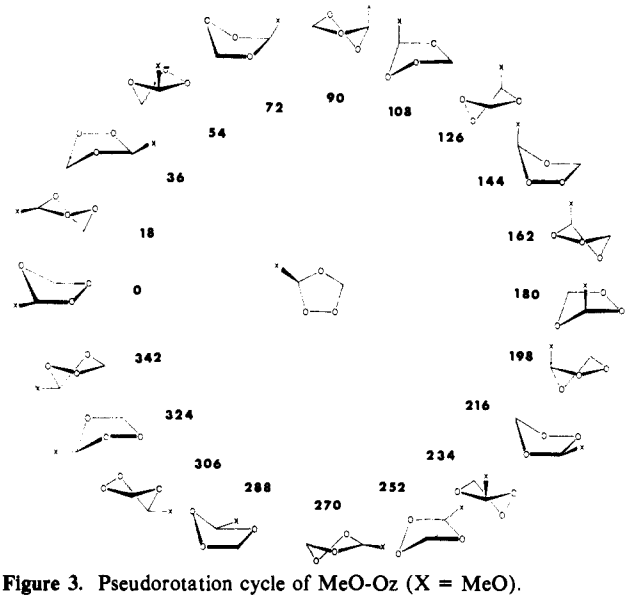

Figure 3. Pseudorotation cycle of MeO-Oz (X = MeO).

Discussion

The structure of MeO-Oz depicted in Figures 1 and 2 has several interesting features. The most apparent is the axial methoxy orientation and peroxy envelope conformation where O_4 is puckered above the plane formed by the other ring atoms

(45) Conversion factor AI_a = 505379.05 MHz amu Å^2.
(46) Costain, C. C. *J. Chem. Phys.* **1958**, *29*, 864.

Table VI. Ab Initio Energies for Conformations **1**, **2**, and **3** of the Methoxy Group[a]

basis		conformatn, τ(8,1,6,7)	q	ϕ	abs energy	rel energy
STO-3G	1	52.3	0.389	83.7	−411.067 86	0.41
	2	178.6	0.375	73.4	−411.068 52	0
	3	304.3	0.388	84.1	−411.067 28	0.78
4-31G	1	56.9	0.387	101.8	−415.794 28	2.16
	2	179.8	0.385	77.4	−415.797 72	0
	3	300.2	0.386	94.6	−415.792 83	3.07
6-31G*[b]	2	180.2	0.385	77.4	−416.412 62	

[a] Absolute energies in hartree, relative energies in kcal/mol, puckering amplitude q in Å, dihedral angle and pseudorotation phase angle in deg. [b] 4-31G geometry used.

($\tau(O_5-C_1-O_2-C_3)$ = 1.4°). The experimentally determined pseudorotation phase angle ϕ is 70°, which is just 2° below the value of an ideal peroxy envelope[47] (compare with Figure 3). The conformation of MeO-Oz is similar to the one found for vinylidene fluoride ozonide (1,1-F_2Oz, ϕ = 67°)[47] where the puckering of the O–O group enhances the anomeric interaction involving the fluorine atoms and the oxygens in the ring.[18] By analogy, an anomeric interaction must also be present in MeO-Oz involving the axial O_{Me} and one or more of the ring oxygen atoms.

A unique conformational feature is the location of the methyl group over the ring. This is the first clear evidence from structural data for such an orientation for an OR substituent on a heterocyclic ring. Typically in carbohydrates a methyl group in an alkoxy substituent is located gauche to the endocyclic oxygen while trans to the endocyclic carbon placing it outside the ring to minimize steric repulsions with methylene hydrogens. There is evidence based on a combination of dipole moment and NMR data in an analogous five-membered ring compound, 2-methoxy-1,3-dioxolane, that the anti ↔ gauche equilibrium in solution favors the anti conformer placing the methyl group over the ring.[48] The anti conformer **6** possesses two clinal O–C–O–Me arrange-

6 **7**

ments (τ (OC–OMe) = 60°) thought to be more stable than antiperiplanar O–C–O–Me (τ (OC–OMe) = 180°), whereas the gauche conformer **7** contains only one. This is the essence of the exo-anomeric effect.

Although the location of the methyl group in MeO-Oz has been established, there is no microwave data to determine the internal rotation angle $\tau(C_1O_6-C_7H_{11,12,13})$ of this group. The orientation in Figure 2 was chosen since it is suggested by the ab initio calculations (see below) and since it staggers the methyl hydrogen atoms relative to the C_1-O_6 bond and eclipses them with respect to the ring C–O bonds. Furthermore it allows for (attractive) intramolecular H, O interactions as discussed below.

In order to verify these assumptions, shed light on the structural parameters and anomeric effect, and estimate if any other low-energy conformers may have been overlooked in the spectroscopic study, an independent determination of the equilibrium geometry of MeO-Oz with the aid of ab initio calculations has been carried out. In Table VI, theoretical energies and conformational data of the three most stable forms of MeO-Oz (**1**, **2**, and **3**) are given. These forms are encountered upon rotation of the MeO group from $\tau(H_8C_1-O_6C_7)$ = τ = 0–360°. They correspond to exo positions of Me with $\tau \approx 60°$ (form **1**) or $\tau \approx 300°$ ($\approx -60°$) (**3**) and to the endo position of Me with τ close to 180° (**2**). The latter is equivalent to the conformation experimentally observed and is shown in Figures 2 and 3. **2** is located at the global minimum of the energy hypersurface of MeO-Oz while **1** and **3** correspond to local minima of the hypersurface.

Table VII. Comparison of Ozonide Structures[a]

param[b]	EtOZ, X = H	FOz, X = F	t-F_2Oz, X = F	1,1-F_2Oz, X = F	MeO-Oz, X = OCH_3
O_e-C_X	1.415	1.382	1.401	1.368	1.406
O_e-C_H		1.426		1.425	1.430
O_p-C_X	1.410	1.382	1.368	1.360	1.411
O_p-C_H		1.411		1.404	1.406
O_p-O_p	1.461	1.463	1.455	1.467	1.474
C–X	1.090	1.375	1.366	1.360	1.377
$C-O_e-C$	104.6	105.3	105.3	103.9	105.8
$C_X-O_p-O_p$	99.2	101.1	101.8	101.8	102.9
$C_H-O_p-O_p$		101.1		99.4	99.1
$O_e-C_X-O_p$	105.7	107.6	106.8	110.5	106.3
$O_e-C_H-O_p$		104.6		103.5	103.6
$C-O_p-O_p-C$	49.4	46.0	41.9	42.0	44.9
O_p-O_p-C-X		83.5	84.1	96.0	97.4
$C-O_e-C-X$		110.3	108.0	126.0	127.2
q[c]	0.456	0.431	0.376	0.424	0.435
phase angle, ϕ[c]	90	97	90	67	70

[a] All substituents are axial. EtOz = ethylene ozonide; FOz = vinyl fluoride ozonide; t-F_2Oz = *trans*-difluoroethylene ozonide; 1,1-F_2Oz = vinylidene fluoride ozonide. [b] Bond lengths and puckering amplitude q in Å and angles in deg. O_e = ether oxygen, O_p = peroxy oxygen, C_H = CH_2 carbon, C_X = substituted carbon. [c] For a definition of q (puckering amplitude, Å) and ϕ see: ref 29; see also ref 47.

The HF/4-31G geometry of **2** is listed in Table V along with parameters calculated for **1** and **3**. Theoretical and experimental geometry data are in reasonable agreement. It is well-known[22] that both the STO-3G and the 4-31G basis underestimate the degree of ring puckering considerably (see puckering amplitude q and dihedral angles in Tables V–VII). In addition, the 4-31G basis leads to an overestimation of bond polarities, thus artificially widening COC and COO angles. Nevertheless, ab initio results confirm the experimentally observed conformational features completely. Thus, MeO-Oz adopts the peroxy envelope conformation (ϕ(STO-3G) = 73°, ϕ(4-31G) = 77°, Table VI, compare also with Figure 3) with the MeO substituent in an axial position and the Me group being endo (τ = 180°). In addition, calculations show that the methyl hydrogens are perfectly staggered with regard to the bond C_1-O_6 (see relevant dihedral angles in Table V) and that the staggered conformation is maintained during rotation of the methoxy group or during pseudorotation of the ring. The nonbonded distance C_1, H_{13} is 2.66 Å thus lending support to the corresponding assumptions made when determining the experimental geometry.

It is intriguing to compare structural features of MeO-Oz with those found for other ozonides and to investigate in which way different electronic and steric interactions between substituent and ring influence geometry and conformation. Selected data is summarized in Table VII.

The complete pseudorotational surface of the parent ozonide, EtOz (ethylene ozonide), has been determined by ab initio calculations (see Figure 4 in ref 22). It has been shown that EtOz adopts a twist conformation (ϕ = 90° or 270°), which is more stable than the envelope forms at ϕ = 0° or 180° (Figure 3) by 3 kcal/mol.[22] In the twist form, EtOz has C_2 symmetry, which is reduced to C_1 symmetry upon substitution at a ring carbon. For MeO-Oz one can distinguish between the twist form at ϕ = 90° with the MeO group in an axial position and the twist form at ϕ = 270° with the MeO group in an equatorial position (see Figure 3). Cremer[20-22] has shown that π-donor substituents such as MeO prefer the axial position. In this position, the overlap between the HOMO of the Oz ring, which possesses π character (see Figure 3 in ref 21), and the electron lone pair orbitals of a substituent X (X = MeO) is minimized and, accordingly, destabilizing

(47) Note that the value of the pseudorotation phase angle ϕ depends on the numbering of the ring atoms. In order to directly compare ϕ with the corresponding values of other ozonides (see ref 16, 21, and 22), the ring atoms of MeO-Oz have been renumbered according to the convention given in ref 22 and used in Figure 3, i.e., O_2 is atom 1, C_1 is atom 2, etc. Adopting this numbering for 1,1-F_2Oz, ϕ = 67° is obtained rather than 113° (see Table VII, ref 16).

(48) Altona, C.; Van der Veek, A. P. M. *Tetrahedron* **1968**, *24*, 4377.

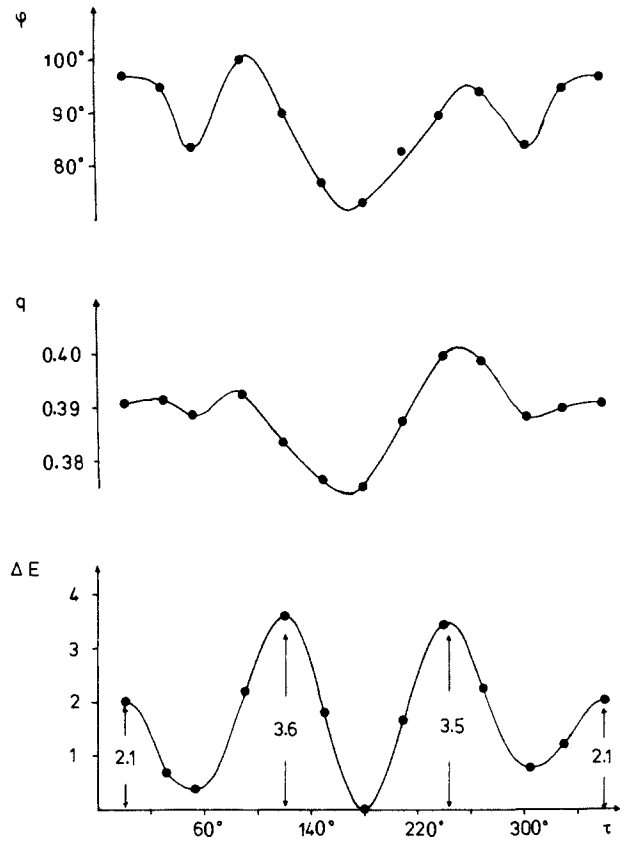

Figure 4. Dependence of the molecular energy ΔE (kcal/mol, relative to the energy of the most stable form **2**), the puckering amplitude q (Å), and the pseudorotation phase angle ϕ (deg) on the rotational angle τ-(H_8C_1–O_6C_7) (HF/STO-3G calculations).

four-electron interactions are largely avoided.[49]

Both experimental and calculated results suggest that MeO-Oz prefers an equilibrium geometry with a pseudorotation phase angle about 20° smaller than that of the twist form at 90°. Ab initio results in Table VI reveal, however, that the pseudorotation phase angle is very sensitive to the conformation of the MeO group. If the MeO group rotates from the more stable endo position (**2**, $\tau \approx 180°$) into one of the exo positions with $\tau \approx 60°$ (**1**) or −60° (**3**), then ϕ will increase to 102° and 95° (HF/4-31G results), respectively, where these conformational changes are accompanied by an increase in q (see also Figure 5). The exo forms **1** and **3** are less stable by 0.4 and 0.8 kcal/mol (HF/STO-3G). The corresponding HF/4-31G energies are considerably higher (2.2 and 3.1 kcal/mol), but this is probably an artifact of the split valence basis.[50]

In Figure 5 the rotational potential of the MeO group is shown as a function of the dihedral angle $\tau(H_8C_1$–$O_6C_7) = \tau$. Rotation of the MeO group into the exo positions requires 3–4 kcal/mol, which is typical of the conformational barriers in methyl alkyl ethers. Variation of the pseudorotational angle ϕ and the puckering amplitude q with τ are also shown in Figure 5.

An interesting feature in MeO-Oz is the shortening of the C–OMe bond relative to the ring bonds C_1–O_5 and C_1–O_2 in both the experimentally and theoretically derived structures. This differentiation in bond length at the anomeric center is also a manifestation of the exo-anomeric effect as observed in alkyl pyranosides and most recently in a novel bicyclic alkoxy ozonide.[25] In general, pyranose sugars **8** with the general formula $(CH_2)_nXCH_2Y$ where X is oxygen have shortened exocyclic C_1–Y

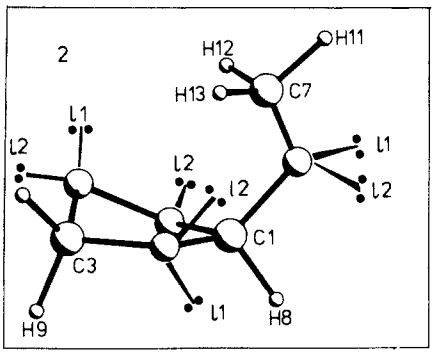

Figure 5. Lone pair numbering. Lone pair $\ell 1$ on the peroxide oxygen is obscured behind the peroxide and ether atoms.

Table VIII. Atomic Charges Calculated at the HF/6-31G* Level of Theory

atom	charge [e]	group	charge [e]
C_1	0.795	C_1H	1.006
C_2	−0.682	$C_3H_{9,10}$	0.696
C_3	0.314	O_4O_5	−0.762
O_4	−0.367	$C_7H_{11,12,13}$	0.367
O_5	−0.395	MeO	−0.259
O_6	−0.626		
C_7	−0.186		

bond lengths when Y is OR and lengthened C_1–Y bond lengths when Y is an axial halogen.

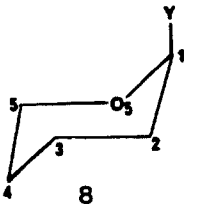

8

Comparison of energies, geometries, and charge distributions for **1**, **2**, and **3** provide a possibility of elucidating in which way the geometrical trends are consequences of anomeric and exo-anomeric effects. The atomic charges listed in Table VIII reveal that C_1, which is bonded to three electronegative O atoms, is highly positively charged (0.795 e). Upon loss of negative charge the covalent radius of an atom normally decreases thus leading to shorter bonds. This effect is well known (compare, e.g., CF bond lengths in CH_3F, CH_2F_2, and CHF_3[51]) and has been described in terms of an increase in the ionic character of the bond CX.[13] In the case of MeO-Oz, only one C_1–O bond is significantly shortened (C_1–O_6), while C_1–O_2 and C_1–O_5 are longer than might be expected in view of the high positive charge of C_1. This, however, can be explained when considering the various anomeric interactions involving ring and substituent orbitals.

The direction of electron lone pair delocalization due to anomeric interactions in a fragment O–C–X depends on the energy of σ^*(C–X) and the overlap between lone pair (ℓ) and σ^* orbitals. For X = F the energy of σ^*(C–X) is lower than that of σ^*(C–O), i.e., electron delocalization will take place from the O lone pair orbital into the exocyclic C–F bond thus leading to a shortening of the C–O bond and a lengthening of the C–F bond. This has been confirmed when determining the geometry of F-substituted ozonides (see Table VII). In these compounds the peroxy group is a stronger π donor than the ether oxygen because of lone pair, lone pair repulsion in the former. For example, in *t*-F_2Oz the bond C–O_p (1.368 Å) is considerably shorter than the bond C–O_e (1.401 Å).[16]

In the case of MeO-Oz, it is difficult to predict the direction of electron lone pair delocalization. However, an analysis of the calculated MOs reveals that the LUMO of MeO-Oz is a σ^*(ring)

(49) Similarly, an electron acceptor substituent prefers an equatorial position since this guarantees maximal HOMO–LUMO overlap between ring and substituent orbitals thus leading to strong stabilizing two-electron interactions.

(50) Since the 4-31G basis overestimates bond polarities and charge separation, anomeric effects and steric interactions are also overestimated (see ref 22).

(51) Yokozeki, A.; Bauer, S. H. *Top. Curr. Chem.* **1975**, *53*, 71.

Chart I Newman Projections at the Bond O_6–C_1[a]

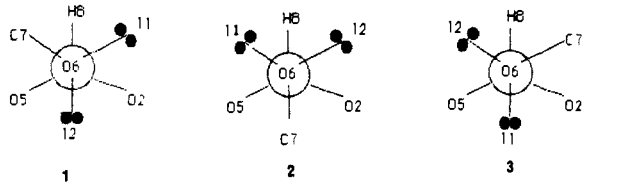

anomeric interactions between

$\ell1$ and $\sigma^*(C_1-O_5)$	$\ell1$ and $\sigma^*(C_1-O_2)$ $\ell2$ and $\sigma^*(C_1-O_5)$	$\ell2$ and $\sigma^*(C_1-O_2)$

consequences

C_1O_6 short:	1.370	C_1O_6 very short:	1.359	C_1O_6 short:	1.371
C_1O_2 normal:	1.396	C_1O_2 long:	1.421	C_1O_2 long:	1.421
C_1O_5 long:	1.435	C_1O_5 long:	1.448	C_1O_5 normal:	1.414

[a] Electron lone pairs are denoted by $\ell1$ and $\ell2$. Anomeric interactions between $\ell1$ or $\ell2$ and adjacent σ^* orbitals are listed, and their consequences with regard to bond lengths are indicated.

MO involving bonds C_1–O_5, C_1–O_2, and O_4–O_5. Accordingly, delocalization of the lone pair electrons at O_6 into σ^*(ring) will be stronger than delocalization of the lone pair electrons at O_2 and O_5 into $\sigma^*(C_1$–$O_6)$.

In Chart I, Newman projections about the bond C_1–O_6 are given for **1**, **2**, and **3**. The positions of the two electron lone pairs at O_6 are indicated assuming sp^3 hybridization at C_1 and O_6. These qualitative descriptions can be improved by investigating the total electron density distribution of $\rho(\mathbf{r})$ and its associated Laplace field $\nabla^2\rho(\mathbf{r})$. While the analysis of $\rho(\mathbf{r})$ provides information about the properties of atoms in molecules and chemical bonds,[52-54] the Laplacian of $\rho(\mathbf{r})$ indicates where the electrons concentrate ($\nabla^2\rho(\mathbf{r}) < 0$) and where they are depleted in a molecule ($\nabla^2\rho(\mathbf{r}) > 0$).[53-55] Concentration lumps in nonbonding regions can be assigned to electron lone pairs and the corresponding position of maximum concentration can be considered as the "position" of the electron lone pair (ℓ).[16]

The electron density distribution $\rho(\mathbf{r})$ and the Laplace concentration $-\nabla^2\rho(\mathbf{r})$ of **2** have been calculated at the HF/6-31G* level of theory, and all lone pair positions have been determined. The corresponding positional data are listed in Table IX. According to these data, $\ell1(O_6)$ and $\ell2(O_6)$ (for definition of $\ell1$ and $\ell2$ see Figure 5) are antiperiplanar with regard to bonds C_1–O_2 (τ = −169.6°) and C_1–O_5 (τ = 173.5°, Table IX), respectively. Hence, two exo-anomeric stabilizing interactions are possible in **2** as indicated in Chart I. For **1** and **3**, there is just one exo-anomeric interaction possible involving either $\ell1$ and $\sigma^*(C_1$–$O_5)$ or $\ell2$ and $\sigma^*(C_1$–$O_2)$. As a consequence, **2** is more stable than **1** or **3**. Furthermore, the bond C_1–O_6, which is already short because of the high positive charge of C_1, becomes even shorter in **2** due to two exo-anomeric interactions. For the same reason C_1–O_2 and C_1–O_5 are lengthened in **2**.

Since only one electron lone pair, either $\ell1$ or $\ell2$, is involved in the exo-anomeric interactions of the exo forms, a less pronounced shortening of bond C_1–O_6 is observed for **1** and **3** (Chart I and Table V). In **1**, bond C_1–O_2 and in **3** bond C_1–O_5 are not affected by exo-anomeric interactions while C_1–O_5 of **1** and C_1–O_2 of **3** are lengthened due to charge transfer into the σ^*(ring) MO. The calculated bond lengths of **1** and **3** (Chart I) indicate that the exo-anomeric effect entails a lengthening of 0.02–0.03 Å in the ring bonds C_1–O_2 and C_1–O_5 and a shortening of similar magnitude in the bond C_1–O_6.

Table IX. Description of Electron Lone Pair Concentrations in Terms of the Laplacian of $\rho(\mathbf{r})$ Calculated at the HF/6-31G* Level[a]

atom	param	lone pair $\ell1$	lone pair $\ell2$
O_6	$r(6,\ell)$	0.335	0.335
	$\alpha(1,6,\ell)$	102.0	101.8
	$\alpha(7,6,\ell)$	103.2	102.5
	$\tau(2,1,6,\ell)$	−169.6	56.2
	$\tau(5,1,6,\ell)$	−52.3	173.5
	$\tau(8,1,6,\ell)$	66.4	−67.8
	$-\nabla^2\rho(\mathbf{r})$	157.6	156.6
O_2	$r(2,\ell)$	0.334	0.334
	$\alpha(1,2,\ell)$	101.1	100.0
	$\alpha(3,2,\ell)$	101.7	100.8
	$\tau(5,1,2,\ell)$	103.5	−108.9
	$\tau(6,1,2,\ell)$	−133.2	14.4
	$\tau(8,1,2,\ell)$	−11.0	136.6
	$\tau(4,3,2,\ell)$	−128.6	82.8
	$-\nabla^2\rho(\mathbf{r})$	161.0	162.0
O_4	$r(4,\ell)$	0.329	0.329
	$\alpha(3,4,\ell)$	98.6	101.2
	$\alpha(5,4,\ell)$	97.9	96.7
	$\tau(2,3,4,\ell)$	−62.1	143.8
	$-\nabla^2\rho(\mathbf{r})$	203.2	200.1
O_5	$r(5,\ell)$	0.329	0.329
	$\alpha(1,5,\ell)$	98.8	100.5
	$\alpha(4,5,\ell)$	97.5	97.2
	$\tau(2,1,5,\ell)$	−72.9	127.6
	$\tau(6,1,5,\ell)$	164.4	4.9
	$\tau(8,1,5,\ell)$	44.9	−114.6
	$\tau(3,4,5,\ell)$	60.3	−143.7
	$-\nabla^2\rho(\mathbf{r})$	199.3	197.0

[a] Lone pairs $\ell1$ and $\ell2$ are given for each atom in Figure 5. Distance r in Å, angles α and τ in deg, $-\nabla^2\rho(\mathbf{r})$ in e/Å^5.

Table X. Close Intramolecular Contacts between Methyl Hydrogens and O Atoms of Ring[a]

conformatn $\tau(8,1,6,7)$	atom	O_2	O_4	O_5
56.9	H_{13}			2.681
179.8	H_{12}		2.750	2.737
	H_{13}	2.647		
300.3	H_{12}	2.669		

[a] Distances in Å. Only nonbonded distances smaller than 3 Å are given.

A comparison of the O–O bond lengths between MeO-Oz and fluoroozonides also suggests that O_p in the former is a weaker π-donor than O_{Me}. The O_p–O_p distance in MeO-Oz is longer by about 0.01–0.02 Å compared to EtOZ, FOz, and *t*-F_2Oz (Table VII). This also suggests more lone pair, lone pair repulsion between adjacent O_p atoms in MeO-Oz consistent with their weaker π donor abilities relative to the exocyclic O_{Me}.

Apart from stabilizing anomeric interactions, electrostatic attraction between the negatively charged O atoms of the ring and the positively charged H atoms of the Me group influence the relative stabilities of **1**, **2**, and **3**. In Table X, nonbonded distances between these atoms are listed. They reveal that in **2** there are three close H, O contacts while there is only one in either **1** or **3**. Again, this leads to a greater stability of the endo form **2**.

In conclusion, the two-pronged investigation of MeO-Oz has revealed a number of interesting structural and electronic features caused by substituent, ring interactions in this substituted ozonide. MW experiments and ab initio calculations show that MeO-Oz in its equilibrium geometry prefers: (a) the peroxy envelope conformation (ϕ = 72°), (b) an axial position of the MeO substituent, (c) an endo position of the Me group, and (d) staggering of the methyl hydrogens with regard to the C–OMe bond.

These preferences are caused or at least influenced by an exo-anomeric effect involving the electron lone pairs at O_{Me} and the C_1–O ring bonds. The exo-anomeric effect is also responsible

(52) (a) Bader, R. F. W.; Slee, T. S.; Cremer, D.; Kraka, E. *J. Am. Chem. Soc.* **1983**, *105*, 5061. (b) Cremer, D.; Kraka, E.; Slee, T. S.; Bader, R. F. W.; Lau, C. D. H.; Nguyen-Dang, T. T.; MacDougall, P. S. *J. Am. Chem. Soc.* **1983**, *105*, 5069. (c) Cremer, D.; Kraka, E. *J. Am. Chem. Soc.* **1985**, *107*, 3800, 3811.
(53) Cremer, D.; Kraka, E. *Croat. Chem. Acta* **1984**, *57*, 1259.
(54) Cremer, D. In *Modelling of Structure and Properties of Molecules*; Maksic, Z. B., Ed.; Ellis Horwood: Chichester, England, 1987; in press.
(55) (a) Bader, R. F. W.; Essén, H. *J. Chem. Phys.* **1984**, *80*, 1943. (b) Bader, R. F. W.; MacDougall, P. J.; Lau, C. D. H. *J. Am. Chem. Soc.* **1984**, *106*, 1594.

for a pronounced shortening of the C_1-OCH_3 bond. This shortening is increased by Coulomb effects involving the strongly positively charged C_1 atom and the three adjacent O atoms. Electrostatic effects between methyl hydrogens and the O atoms of the ring also play a role since they add to the stability of the endo form.

Acknowledgment. This work was supported by Grants CHE-8303615 and CHE-8603834 from the National Science Foundation. Support at the Universität Köln was provided by the Deutsche Forschungsgemeinschaft and the Fonds der Chemischen Industrie. Helpful discussions on various aspects of this research with Dr. Kurt W. Hillig II are gratefully acknowledged. We thank Professor H. D. Rudolph and Dr. V. Typke of Ulm University for the program ZFAP6 which was invaluable throughout this entire project.

Supplementary Material Available: Tables S1-S17 listing transition frequencies and centrifugal distortion constants for the ground vibrational states of the normal and isotopic species and observed and calculated Stark coefficients (18 pages). Ordering information is given on any current masthead page.

Transition Structures for Homodienyl 1,5-Sigmatropic Hydrogen Shifts: Origin of the High Endo Stereoselectivity

Richard J. Loncharich and K. N. Houk*

Contribution from the Department of Chemistry and Biochemistry, University of California, Los Angeles, Los Angeles, California 90024-1569. *Received August 17, 1987*

Abstract: The endo and exo transition structures for the homodienyl hydrogen shift of 1-methyl-2-vinylcyclopropane have been obtained with ab initio quantum mechanical calculations. The difference in energy between the endo and exo transition states is estimated to be 17 kcal/mol, favoring the endo mode of reaction, as compared to Berson's estimate of at least 12 kcal/mol made on the basis of experimental data. The transition structures are compared to that obtained earlier for the simplest ene reaction of propene with ethylene. Orbital overlap factors, which lead to the endo preference, are discussed.

The best understood stereoelectronic imperative is that developed by Woodward and Hoffmann, differentiating thermally allowed and forbidden reactions.[1] Among the thermally allowed pericyclic reactions, there are stereoisomeric variants that have activation energy differences as large as those between allowed and forbidden reactions.[2] These are understood in a few cases, but general rules have not yet emerged. We have been investigating such reactions theoretically, and here we describe theoretical studies of an especially well-documented spectacular reaction of this type.

In connection with our study of the ene reaction,[3] we have undertaken a study of the intramolecular retro-ene reaction of *cis*-1-methyl-2-vinylcyclopropane (**1**). This transformation is also known as the homodienyl 1,5-hydrogen shift. It can occur in two stereochemically distinct modes, endo or exo, both of which are thermally allowed. The endo transition state gives *cis*-1,4-hexadiene (**2**) while the exo transition state gives *trans*-1,4-hexadiene (**3**), as shown in Scheme I. Daub and Berson[4] estimated that the endo transition state is at least 12 kcal/mol lower in energy than the exo transition state. This free energy difference was estimated from experiments on substituted derivatives. Activation energies were measured for compounds having *tert*-butyl substitution at the terminal vinyl position of 1,1-dimethyl-2-vinylcyclopropane (**4**). The trans-substituted system (**4**, R_2 = *t*-Bu) leads to a 7.0 kcal/mol lower activation energy than the *cis-tert*-butyl system (**4**, R_1 = *t*-Bu), which corresponds to a $\Delta\Delta G^{\ddagger}$ of 6.5 kcal/mol; and the *cis-tert*-butyl system gives a cis to trans product ratio of 99.4:0.6, which corresponds to a $\Delta\Delta G^{\ddagger}$ of 5.5 kcal/mol. Thus, the formation of the cis product occurs with a rate that is over 5 orders of magnitude faster than the rate of formation of the trans product. Berson, following an earlier suggestion by Winstein,[5] proposed that this rate difference "is

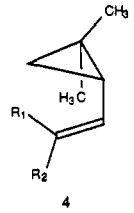

4

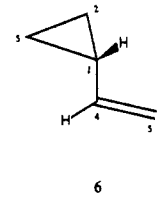

6

Scheme I

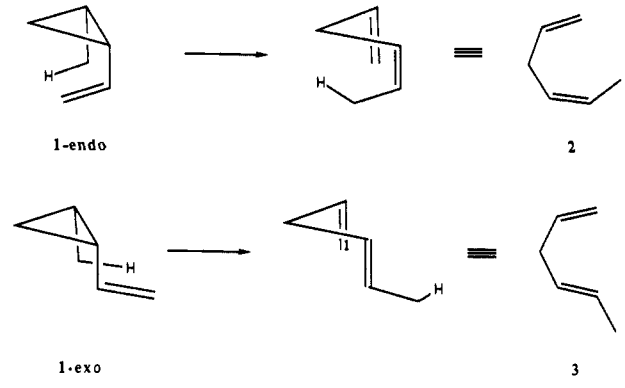

1-endo 2

1-exo 3

Table I. Energetics of the Retro-Ene Reactions of *cis*-1-Methyl-2-vinylcyclopropane (Theoretical Results Are Obtained with the 3-21G Basis Set)[a]

adduct	E_a	$\Delta H^{\ddagger}$	$\Delta S^{\ddagger}$	ΔH_{rxn}	T, K
endo	48.8	45.3	-6.4	-11.0	
exo	65.9	62.0	-6.1	-12.7	
exptl I[b]	31.3			-5.2[c]	543
exptl II[d]	31.2 ± 0.7		-4.7		439-493
exptl III[e]	31.1	30.2 ± 0.6	-3.7		443-463

[a] Absolute energies (au) of the reactant, endo transition structure, exo transition structure, cis product, and trans product are -231.675 44, -231.596 70, -231.570 47, -231.693 02, and -231.695 72, respectively. [b] Reference 4. [c] Reference 10. [d] Reference 8c,d. [e] Reference 8b.

(1) Woodward, R. B.; Hoffmann, R. *The Conservation of Orbital Symmetry*, Academic: New York, **1970**.
(2) See, for example: (a) Rondan, N. G.; Houk, K. N. *J. Am. Chem. Soc.* **1985**, *107*, 2099. (b) Kirmse, W.; Rondan, N. G.; Houk, K. N. *J. Am. Chem. Soc.* **1984**, *106*, 7989.
(3) Loncharich, R. J.; Houk, K. N. *J. Am. Chem. Soc.* **1987**, *109*, 6947.
(4) Daub, J. P.; Berson, J. A. *Tetrahedron Lett.* **1984**, *25*, 4463.

0002-7863/88/1510-2089$01.50/0